IET Renewable Power Generation

Research Article

IET Journals
The Institution of Engineering and Technology

Intelligent grid interfaced solar water pumping system

ISSN 1752-1416
Received on 23rd June 2016
Revised 31st October 2016
Accepted on 5th December 2016
E-First on 10th February 2017
doi: 10.1049/iet-rpg.2016.0597
www.ietdl.org

Utkarsh Sharma[1] ✉, *Bhim Singh*[1], *Shailendra Kumar*[1]

[1]*Department of Electrical Engineering, Indian Institute of Technology Delhi, New Delhi, India*

✉ *E-mail: utkarsh.kota@hotmail.com*

Abstract: This study proposes a solar photovoltaic (SPV) water pumping system integrated with the single phase distribution system by utilising induction motor drive (IMD) with an intelligent power sharing concept. In addition to the power exchange from SPV to the IMD, a DC–DC boost converter is utilised as a power factor correction unit and a grid interfacing device. For good utilisation of SPV array, it is necessary to extract maximum power from the SPV array. To meet this objective, an incremental conductance based maximum power point tracking control is implemented. Whereas, to control the IMD tied to voltage source inverter, a simple voltage/frequency control technique is used. The proposed topology is designed and tested in the laboratory under standalone, grid interfaced and in mixed mode under various operating conditions.

1 Introduction

With the growing demand of energy throughout the world, solar photovoltaic (SPV) based electricity generation is taking lead amongst non-conventional sources of energy [1]. The SPV energy is significantly promising and suitable technology for smart grid formation with distributed network. In the upcoming years, the overall cost of the PV cells is expected to go down drastically.

Water is required for drinking, irrigation, domestic use, for livestock and for industrial use. Water pumping has become an indispensable task in day to day life. Efforts are being made to harvest the solar power for pumping [2]. The hybrid water pumping systems [3] are gaining popularity day by day with smart sharing power concept. Moreover, SPV grid interfaced water pumping system is a cost effective solution as it does not uses any storage (batteries) system. In standalone SPV systems, energy storage devices (batteries) have been utilised to store the SPV energy. The standalone SPV fed water pumping system with an energy storage system is reported in [4]. There are many complications with batteries such as low life, hazardous waste and acid leakage in lead acid batteries. For these reasons, grid supported SPV water pumping systems are preferred over the battery supported systems where the grid supply is available [5]. A hybrid water pump is presented in [6] which is able to draw power either from the SPV array or from the single phase grid. However, a transformer is used to feed the power from the inverter to the pump. The transformer is a bulky and costly equipment. This makes the whole system unsuitable for pumping with high power requirements. A high value inductor of the rating 185 mH is used in line to interface the transformer and the pump. Such high inductor rating is infeasible for agricultural and irrigation products. Many researchers have proposed standalone water pumps [7–10] which do not have grid interaction and power quality improvement features. A water pumping system powered with wind energy conversion system (WECS), SPV array and battery is discussed in [11]. Self-excited induction generators use capacitors for meeting reactive power requirements. Capacitors form the most unreliable component of the whole system. Moreover, the WECS are suitable for high power generation systems. For small capacity pumps under 10 hp, WECS may not find justification for capital investment.

For extraction of variable power from the SPV array efficiently, a floating step size incremental conductance (INC) based maximum power point tracking (MPPT) has been reported in [12]. Many researchers have proposed the INC based control technique with its merits and demerits [13, 14]. It states that among all MPPT techniques, an INC based MPPT is simple to handle and it has good tracking efficiency. Moreover, it also adjusts the step size automatically to reach the MPP and improves the response under steady state and dynamic conditions. Moon *et al.* [15] have proposed a new MPPT technique to fulfil these objectives of MPPT. The technique uses only one sensor as compared to multi sensor scheme and is able to track the MPP efficiently. A technique to reduce the steady state losses at MPP has been proposed in [16] which embodies idle operation at MPP. Moreover, nature inspired meta heuristic algorithms have been used to track the MPP [17]. However, the performance of such algorithms diminishes during transients due to complexity of the algorithm. Improvements in INC algorithm have been suggested by wisely updating the duty ratio of boost converter considering the LC resonance in [18].

Now a days, large induction motor drives (IMDs) and power converters connected to the distribution network are the main cause for the power quality deterioration. Industries, commercial establishments and households are subjected to poor power quality due to the large IMDs connected at point of common coupling. Besides operation of large IMDs, utility voltage distortion and unbalancing operation also deteriorate the power quality of distribution system [19]. A power factor controlling unit with front end rectifier for IMD have been discussed in [20]. The proposed topology works well as power factor correction (PFC) unit whereas, power sharing from the renewable energy sources has not been discussed. The power factor and efficiency improvement with novel concept of the IMD are discussed in [21, 22]. Again the reported literature has focused on efficiency and power factor improvement. There is no discussion on power sharing concept with different sources. A DC–DC boost converter is utilised for PFC and for maintaining the DC bus voltage [23]. Power factor improvement with the help of boost converter is reported in [24, 25]. However, the controller used in the reported literature are very complex and computational burden is also high. It is demonstrated in the experimental results that the control of boost converter keeps the grid current total harmonic distortion (THD) below the value as per IEEE-519 standard [26]. A Cuk converter is used to improve the power factor of BLDC motor drive in [27].

This paper deals with the design, control and implementation of a grid interfaced unidirectional SPV fed water pumping system. The paper introduces the need of SPV based water pumping system and available literature. The rest of the paper is organised as follows. The system configuration is described in Section 2. Various design parameters and considerations are given in Section

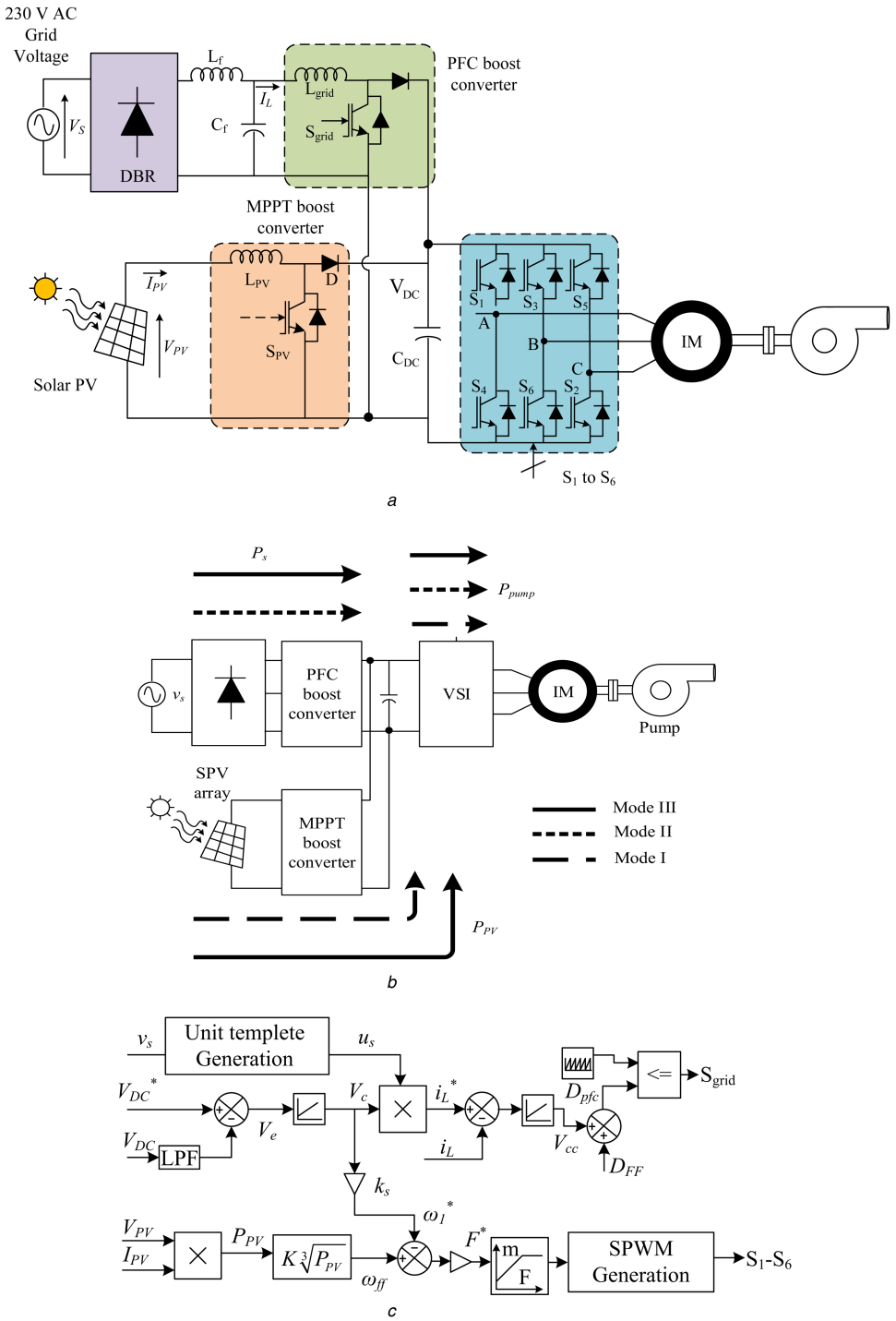

Fig. 1 *System configuration, mode of operation and control scheme of the proposed system*

(a) System configuration for the proposed intelligent grid interfaced solar water pumping system, ***(b)*** Power flow in difference modes of operation, ***(c)*** Control scheme for proposed grid interfaced water pumping system

3. Section 4 presents the control scheme used for proposed system. The simulated and experimental results with their analysis of the proposed system are presented in Sections 5 and 6, respectively. It is concluded in Section 7.

2 Configuration of system

Fig. 1*a* describes the system configuration for the proposed intelligent grid interfaced SPV fed water pumping system. The system consists of an IMD based pump, a SPV array, three power converters [two boost converters and one voltage source inverter (VSI)], and one diode bridge rectifier (DBR). VSI is used to provide pulse width modulated AC voltage to the IMD. The grid side boost converter is used to step up the voltage from rectified grid voltage to the reference DC link voltage as well as for PFC at AC mains. The SPV boost converter is used for MPPT of SPV array. An L-C based EMI filter is connected at the output of DBR to eliminate the high switching ripple in AC mains. The data of the motor are given in Appendix.

3 Design of proposed system

The system shown in Fig. 1*a* incorporates a SPV array, two boost converters, a VSI and motor pump assembly. An induction motor of 2.2 kW rating is selected for simulation as well as experimental validation of the system. The designed values for the proposed system configuration are described in following section.

For satisfactory operation of the pump, a SPV array rated for 2.3 kW is designed using LG210P1C-G2 modules. The peak power rating of individual module is 210 W. The rating of the SPV array

is selected higher than the rated capacity of the motor to compensate for the losses occurring in the VSI, motor and the pump. The DC bus voltage is selected as 400 V. The electrical specifications of the individual solar module and the designed array are given in Table 1.

A centrifugal pump is coupled to the shaft of the submersible induction motor for water pumping. The pump constant is derived using the affinity law of pumps [28] as

$$K_{\text{pump}} = \frac{T_e}{\omega^2} = \frac{14.69}{149.7^3} = 6.55 \times 10^{-4} \quad (1)$$

The design of the system parameters and values of passive components are tabulated in Table 2.

4 Control of proposed system

A smart power sharing scheme between the two power sources is implemented. Whatever maximum energy from SPV array is available is given priority over the grid power on account of its negligible cost. The system uses two boost converters, one for MPPT operation of a SPV array and other for PFC of the AC mains current. An INC algorithm is used for the MPPT while a closed loop current control is used for PFC operation in continuous conduction mode (CCM).

On the basis of power source availability, the proposed system is controlled in three different modes. These modes are explained as follows.

Mode I: In presence of solar power for stand-alone operation, Mode I operates. The boost converter at PV side increases the PV voltage from V_{mp} to reference voltage at DC bus while maintaining the PV operating point at MPP. The DC bus voltage is maintained by PI controller which sets the reference speed/frequency of IMD. As the power output is proportional to the speed of IMD, if there is an increase in the DC bus voltage from the reference value, excess power is fed into the pump by increasing the speed and vice versa holds true.

Mode II: This mode operates when solar panels are disconnected or sufficient radiation is not available, for example during night time. Single phase grid supply is connected to a DBR, followed by a boost converter, DC link capacitor, VSI and an induction motor. The current drawn by a diode bridge rectifier with DC link capacitor is highly distorted and is not allowed according to IEEE 519 standard. With a PFC boost converter, the system is able to draw a sinusoidal current from AC mains. In this mode, the motor runs at the rated speed and gives a rated water discharge.

Mode III: This mode is in operation when the power from both SPV array and grid are available. IMD extracts the maximum available power from the PV source, while taking the deficit power from the grid supply. Under this mode, the system consumes much less power from the grid even at rated discharge, thereby reducing the burden on the grid. Moreover, PFC boost converter is functional and keeps the THD of AC mains current under allowable limits. Fig. 1*b* depicts the direction of power flow in the three modes. The pump gives the rated discharge in this mode.

Table 1 Design of SPV array

Parameter	Specification
name of solar module	LG Electronics LG210P1C-G2
maximum power of module	210 W
open circuit voltage and short circuit current of module	35.7 V and 7.99 A
MPP voltage and current of module	28.7 V and 7.32 A
cells per module	60
maximum power of SPV array	2.3 kW
open circuit voltage and Short circuit current of SPV array	392.7 V and 7.99 A
voltage and current of SPV array at MPP	315.7 V and 7.32 A
no. of modules connected in series and parallel	11 and 1

4.1 Maximum power point tracking algorithm

For MPPT operation of the SPV array, an incremental conductance method (INC) is utilised [30]. Input signals, V_{PV} and I_{PV} are used to estimate the duty ratio of the boost converter for transfer of maximum power. An incremental conductance is calculated from the sampled values of V_{PV} and I_{PV} at kth and $(k-1)$th instants. The equations stating the region in which SPV array operates are as

$$\frac{\Delta I_{\text{PV}}}{\Delta V_{\text{PV}}} = \frac{-I_{\text{PV}}}{V_{\text{PV}}}, \quad \text{at MPP} \quad (2a)$$

$$\frac{\Delta I_{\text{PV}}}{\Delta V_{\text{PV}}} > \frac{-I_{\text{PV}}}{V_{\text{PV}}}, \quad \text{to the left of MPP} \quad (2b)$$

$$\frac{\Delta I_{\text{PV}}}{\Delta V_{\text{PV}}} < \frac{-I_{\text{PV}}}{V_{\text{PV}}}, \quad \text{to the right of MPP} \quad (2c)$$

For satisfactory tracking of the MPP, the reference duty ratio signal is perturbed. The duty ratio is varied as

Table 2 Design of parameters of the system

Component/parameter	Expression	Data input	Calculated value	Used value
V^*_{DC}	$V_{\text{DC}} = \frac{2\sqrt{2}V_{LL}}{\sqrt{3}}$	V_{LL} = 230 V	375.6 V	400 V
C_{DC}	$C_{\text{DC}} = \frac{6\alpha V_{LL} It}{[V^{*2}_{\text{DC}} - V^2_{\text{DC1}}]}$	α = 1.2V^*_{DC} = 400 VV^1_{DC} = 375 VV_{LL} = 133 I = 8.3 At = 0.005 s	2051 μF	2200 μF
D_{PV}	$D = \frac{V_{\text{DC}} - V_{mp}}{V_{\text{DC}}}$	V_{DC} = 400 VV_{mp} = 315.7 V	0.21	0.21
L_{PV}	$L_{\text{PV}} = \frac{V_{mp}D}{\Delta I_1 f_{\text{s}}}$	V_{mp} = 315.7 VD = 0.21 ΔI = 1.464 Af_{s} =	4.52 mH	5 mH
L_{grid}	$L_{\text{grid}} = \frac{V_{\text{DC}}D_a(1-D_a)}{f_{\text{sw}}\Delta I_L}$	V_{DC} = 400 VΔI_L = 3.08 AV_s = 230 Af_{s} = 10 kHz	1.97 mH	3 mH
$C_{f\max}$ [29]	$C_{f\max} = \frac{I_p \tan(\theta)}{2\times\pi\times f\times V_p}$	I_p = 15.42 AV_p = 325.26 Vθ = 1°f = 50 Hz	2.63 μF	2.5 μF
L_f [29]	$L_f = \frac{1}{4\times\pi^2\times f_{\text{c}}^2\times C_f}$	C_f = 2.5 μFf_{c} = 2 kHz	2.53 mH	2.5 mH

$$D_{\text{ref}}(k)=\begin{cases} D_{\text{ref}}(k-1) & \text{if} \quad \dfrac{\Delta I_{\text{PV}}}{\Delta V_{\text{PV}}}=\dfrac{-I_{\text{PV}}}{V_{\text{PV}}} \\ D_{\text{ref}}(k-1)-\Delta D & \text{if} \quad \dfrac{\Delta I_{\text{PV}}}{\Delta V_{\text{PV}}}>\dfrac{-I_{\text{PV}}}{V_{\text{PV}}} \\ D_{\text{ref}}(k-1)+\Delta D & \text{if} \quad \dfrac{\Delta I_{\text{PV}}}{\Delta V_{\text{PV}}}<\dfrac{-I_{\text{PV}}}{V_{\text{PV}}} \end{cases} \tag{3}$$

4.2 Control of induction motor drive

An IMD is controlled using the scalar or V/f control algorithm. A PI controller is used to control the DC link voltage. A feed-forward term is calculated from the power output from the PV source using the pump's law and added to the PI controller's output. The sum of the two quantities is the reference speed for satisfactory performance of IMD with MPPT. The feed-forward term reduces the burden on PI controller and helps to improve the dynamic characteristics of the system. Generated reference speed is given to the scalar control block which determines the switching pulses for the VSI. At starting, the speed is ramped from standstill condition, to a particular threshold. Thereafter, the reference speed is calculated from above mentioned control scheme. Fig. 1*c* shows the control block diagram for the grid interfaced SPV water pumping system.

The reference speed for the induction motor is calculated as follows.

$$P_{\text{PV}}=V_{\text{PV}}\times I_{\text{PV}} \tag{4}$$

$$\omega_{\text{ff}}=K\times\sqrt[3]{P_{\text{PV}}} \tag{5}$$

where, ω_{ff} is the feed forward term. It reduces the burden on the DC link PI controller. An error V_{e} in the DC bus voltage is obtained by subtracting the actual DC bus voltage V_{DC} from the reference DC bus voltage V_{DC}* as

$$V_{\text{e}}(k)=V^{*}_{\text{DC}}(k)-V_{\text{DC}}(k) \tag{6}$$

A proportional-integral (PI) controller is used to minimise this error. The output of the PI controller is a signal V_c which is

$$V_c(k)=V_c(k-1)+k_{\text{p}v}\{V_{\text{e}}(k)-V_{\text{e}}(k-1)\}+k_{\text{i}v}V_{\text{e}}(k) \tag{7}$$

where, $k_{\text{p}v}$ and $k_{\text{i}v}$ are the gains of the above mentioned PI controller. Moreover, this control voltage is fed to a proportional (P) controller for estimation of signal ω_1*. The resultant reference speed ω* for the induction motor is calculated by subtracting the ω_1* from ω_{ff}.

$$\omega^{*}_{1}=V_c(k)\times k_s \tag{8}$$

$$\omega^{*}=\omega_{\text{ff}}-\omega^{*}_{1} \tag{9}$$

4.3 Power factor correction technique

The power quality of the AC mains current in Mode II and Mode III is poor without any PFC circuit. The boost converter is operated in CCM mode. In CCM mode, the inductor current and output capacitor voltage are continuous throughout the switching period. The closed loop current control scheme is used for PFC operation [31].

A unit template of DBR output is multiplied with the signal V_c to get the reference current as

$$i^{*}_{L}=\left|\frac{v_s(k)}{V_m}\right|V_c(k) \tag{10}$$

An error in the input current is found by subtracting the actual input current from the reference input current i_L* as

$$i_{\text{e}}(k)=i^{*}_{L}(k)-i_L(k) \tag{11}$$

Further, this error is passed on to a PI controller which generates a voltage signal V_{CC} as

$$V_{cc}(k)=V_{cc}(k-1)+k_{\text{p}i}\{i_{\text{e}}(k)-i_{\text{e}}(k-1)\}+k_{ii}i_{\text{e}}(k) \tag{12}$$

where, $k_{\text{p}i}$ and k_{ii} are the gains of the voltage PI controller. This voltage signal, V_{CC} is added with a duty ratio feed forward term D_{FF}. The summed output is given to a triangular PWM generator, to generate the duty ratio for the boost converter.

In a PFC boost converter, the duty ratio is a function of time t and supply frequency ω and duty ratio feed forward term is calculated as

$$D_{\text{FF}}=1-\frac{|V_m\sin(\omega t)|}{V_{\text{DC}}} \tag{13}$$

The final duty ratio for the boost PFC converter is calculated as

$$D_{\text{pfc}}=D_{\text{FF}}+V_{CC} \tag{14}$$

5 Simulated performance of proposed system

The response of the proposed intelligent grid interfaced solar water pumping system is analysed with the help of simulations carried out in MATLAB/Simulink. The starting and steady state performances of the system in three different modes of operation are simulated. Moreover, step and slope changes in solar insolation levels are simulated to examine the operation of the system in the dynamic conditions.

In Fig. 2*a*, the starting characteristics of the pump in Mode I are depicted. The motor is started in soft manner to limit the starting current. After 1200 rpm, the reference speed is calculated by control scheme. At 8.6 s, V_{PV} and I_{PV}, are settled to their MPP values. Further, the DC bus voltage is maintained to reference value of 400 V. A slope decrease in radiation is observed from t = 2 s to 3 s from 800 to 400 W/m^2 in Fig. 2*b*. Similarly an increase in radiation from 400 to 800 W/m^2 is simulated from t = 3 s to 4 s. With a decrease in the insolation, the PV current reduces and the speed of the motor reduces. Moreover, step change in the radiation is shown in the Fig. 2*b* to ensure the quick response of the system. In Fig. 2*c* steady state performance of the system in Mode II is depicted. Since the SPV array is unable to generate power, the system draws rated power from the AC mains. It is clearly, visible from the figure that the grid current has power factor close to unity and it maintains the sinusoidal waveform. The performance of the system in Mode III is shown in Fig. 2*d*. In Fig. 2*d*, the radiation is varied in slopes as well as in step changes. The notable feature of the system in this mode is the intelligent sharing of power which can be observed from these figures. As the radiation is decreased, the system starts drawing required power from the grid to provide the rated discharge. In case of an increase in radiation vice-versa is also true.

6 Experimental validation of proposed system

A prototype is developed in the laboratory to validate the response of the proposed intelligent grid interfaced solar water pumping system. The prototype is made using an induction motor of 2.2 kW rating which is coupled with a DC machine, a SPV simulator (AMETEK ETS 600 × 17DPVF), power converters which include VSI and both the boost converters (Semikron make SKM300GB12V and SKM100GB12V, respectively). The open circuit voltage of the SPV array is selected of the order of 400 V while the short circuit current selected as 7.3 A. A DSP (d-SPACE 1104) controller is used to implement the proposed control scheme and provides the gating pulses to the power converters. Three voltages namely V_{DC}, v_s and V_{PV} are sensed using Hall's effect voltage sensors (LV-25P). Further, two currents namely i_s and I_{PV} are sensed using Hall Effect current sensors (LA-55P). The DC

machine is connected to a resistive load which emulates the characteristics of a volumetric pump. A digital storage oscilloscope (Agilent DSO7014A) is used to record the system indices. Moreover, a harmonic spectrum analyser (Fluke 43b) is used to record the power quality of the input AC mains. The experimental characteristics of the system are explained for different modes of operation in following subsections.

6.1 Performance of the system in Mode I

Test results for the proposed intelligent grid interfaced solar water pumping system in Mode I are shown in Fig. 3. In this mode, IMD is powered only from the SPV array. Fig. 3*a* exhibits the recorded waveforms of the PV voltage, PV current, motor phase current and motor speed i.e. V_{PV}, I_{PV}, i_{ma} and N_r at starting. The speed of the IMD is ramped from zero speed to threshold speed of 1200 rpm, after which, reference speed is calculated from the control block. The motor speed is settled at 1330 rpm in steady state condition. The pulses to the boost converter are off up to 1200 rpm, which means the system operates as a single stage system. After 1200 rpm, the boost converter is turned on and the system works as a two stage system. Figs. 3*b–d* show the captured screenshots of the DSO in steady state condition. V_{PV}, I_{PV}, P_{PV} and N_r in steady state condition are shown in Fig. 3*b* at 800 W/m^2. The power extracted at 800 W/m^2 is 1.9 kW. V_{DC} and i_{ma}, i_{mb} and i_{mc} are the system indices shown in Fig. 3*c*. The motor currents maintain sinusoidal waveshape. Fig. 3*d* shows the voltage across the IGBT module V_{SW} and the current through the boost inductor I_L. The MPP tracking capability of the system can be verified from Figs. 4*a* and *b*. The fall and rise in radiation from 800 to 500 W/m^2 and vice-versa are emulated using the PV simulator. From these figures, it can be observed that the PV current, motor current and motor speed are reduced with a fall in radiation. Moreover, they are increased as the solar radiation increases from 500 to 800 W/m^2. However, there is no significant change in V_{PV}.

6.2 Performance of system in Mode II

In Mode II, the system draws power from the utility grid. The recorded waveforms of the system parameters in Mode II are shown in Figs. 5*a–d*. Fig. 5*a* shows the grid voltage v_s, grid current i_s, DC bus voltage V_{DC} and the motor speed N_r. A unity power factor is maintained at the supply AC mains and the waveshape of grid current i_s is sinusoidal. The IMD runs at the rated speed giving the rated discharge. In Fig. 5*b*, along with the grid voltage and current, current through the PFC boost inductor I_{Lgrid} is shown. The inductor current is continuous in nature which validates the

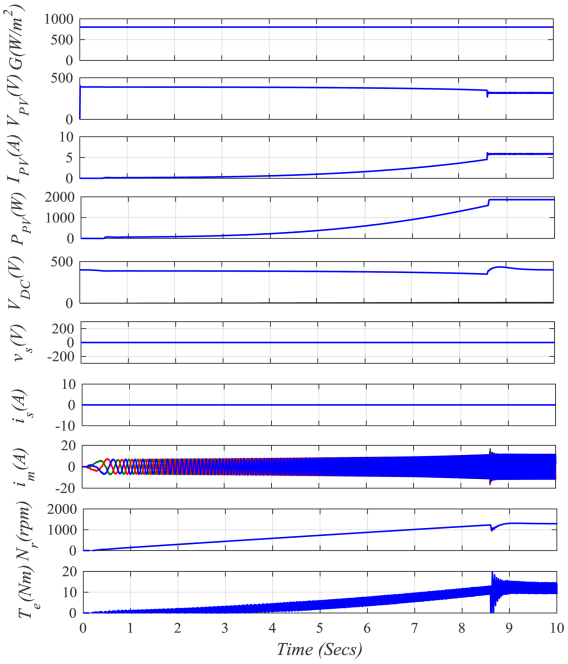

a

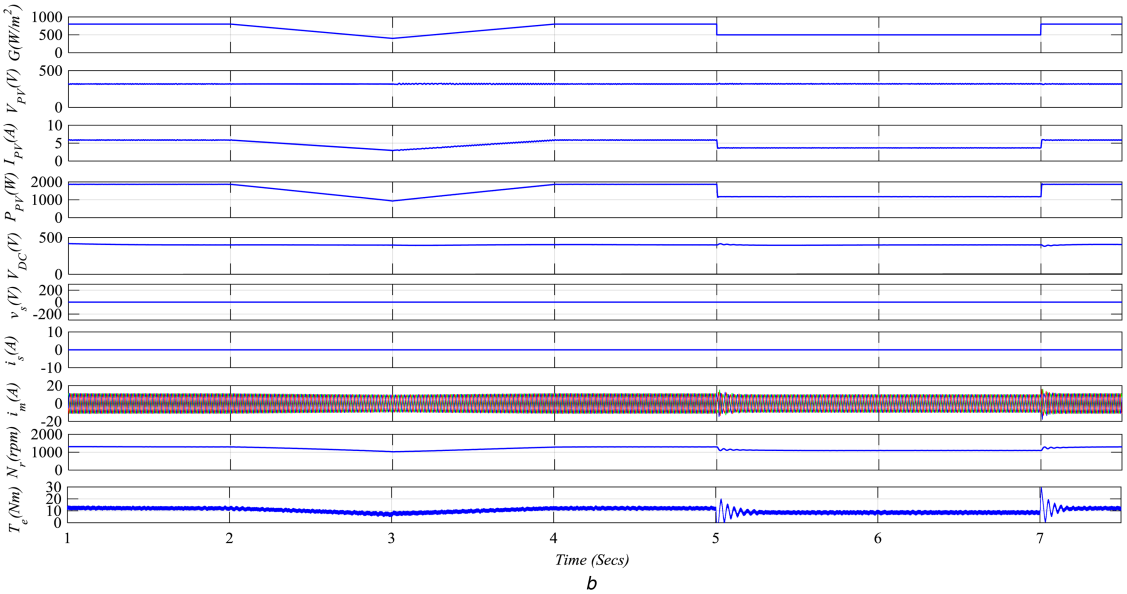

b

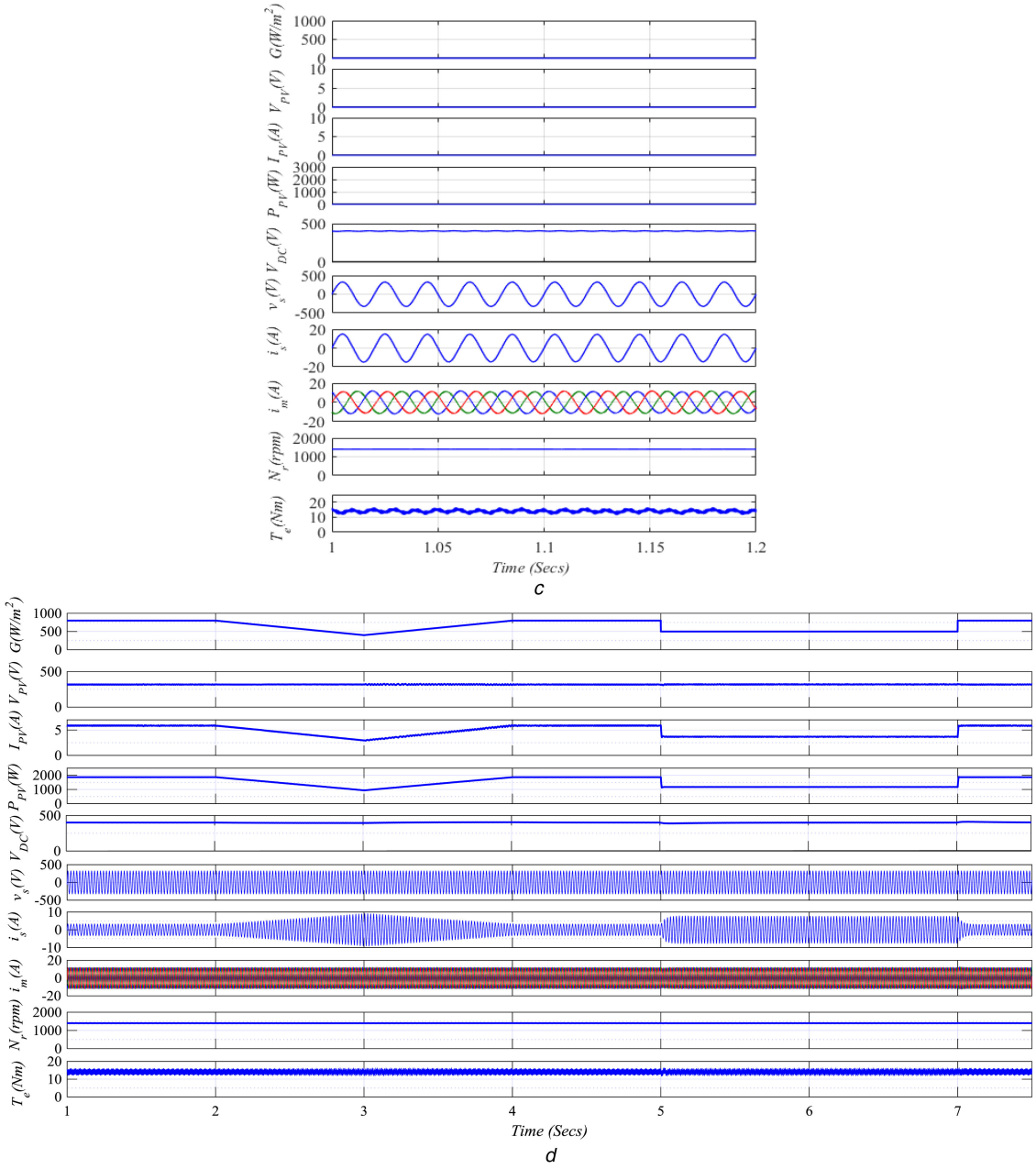

Fig. 2 *Simulated performance of the intelligent grid interfaced solar water pumping system*
(a) Performance of the system in Mode I at starting, ***(b)*** Dynamic performance of the system in Mode I, ***(c)*** Steady state performance of the system in Mode II, ***(d)*** Steady state and dynamic performance of the system in Mode III

CCM operation of the PFC boost converter. The CCM operation of the converter reduces the stress on the switch. The DC bus voltage V_{DC} is maintained to reference voltage of 400 V as observed in Fig. 5*c*. Further, the motor currents i_{ma}, i_{mb} and i_{mc} are maintained sinusoidal. Fig. 5*d* shows the voltage across IGBT switch V_{SWgrid} and the current through PFC boost inductor I_{Lgrid}. Grid parameters at the rated speed are shown in Figs. 6*a*–*c*. The system draws the rated power of 2.42 kW in steady state condition from the utility grid. Moreover, a THD of 3.0% in the grid current is observed which is under the allowable limits of an IEEE 519 standard.

6.3 Performance of system in Mode III

Fig. 7 shows the steady state performance of the system in Mode III. PV voltage, PV current, grid voltage and grid current i.e. V_{PV}, I_{PV}, v_s and i_s are shown in Fig. 7*a* at a radiation of 500 W/m^2. The system draws an active power of 1.31 kW from the grid. In Fig. 7*b*, apart from V_{PV}, I_{PV} and i_s, V_{DC} is shown which is maintained at 400 V level. The similar characteristics are shown in Figs. 7*c* and *d* but with a radiation level of 800 W/m^2. The power available from the PV array is increased, therefore, the active power drawn from the grid is reduced. The supply current in this case i_s is much less than earlier value, thereby confirming intelligent sharing of power between the two sources. Moreover, the V_{DC} is still maintained to 400 V.

Figs. 8*a*–*d* represent the dynamic response of the system under changing solar insolation. A fall in the radiation from 800 to 500 W/m^2 is emulated in Figs. 8*a* and *b*. The PV current I_{PV} decreases and the supply current increases to provide the rated power to the IMD cumulatively. From Fig. 8*b*, it is clearly observed that the speed of the IMD is unaffected by the change in insolation. Further, there is no remarkable perturbation in the PV voltage. In Figs. 8*c* and *d*, the supply current, i_s decreases and PV current, I_{PV} increases with an increase in the solar radiation. Moreover, similar to previous case the motor continues to run with the same speed affirming the uninterrupted water discharge.

The grid supply current i_s along with its harmonic spectrum at solar radiation of 500 and 800 W/m^2 is demonstrated in Fig. 9. In Figs. 9*a* and *b*, it is observed that the current maintains sinusoidal waveform with a THD of 2.9%. The total power drawn from the

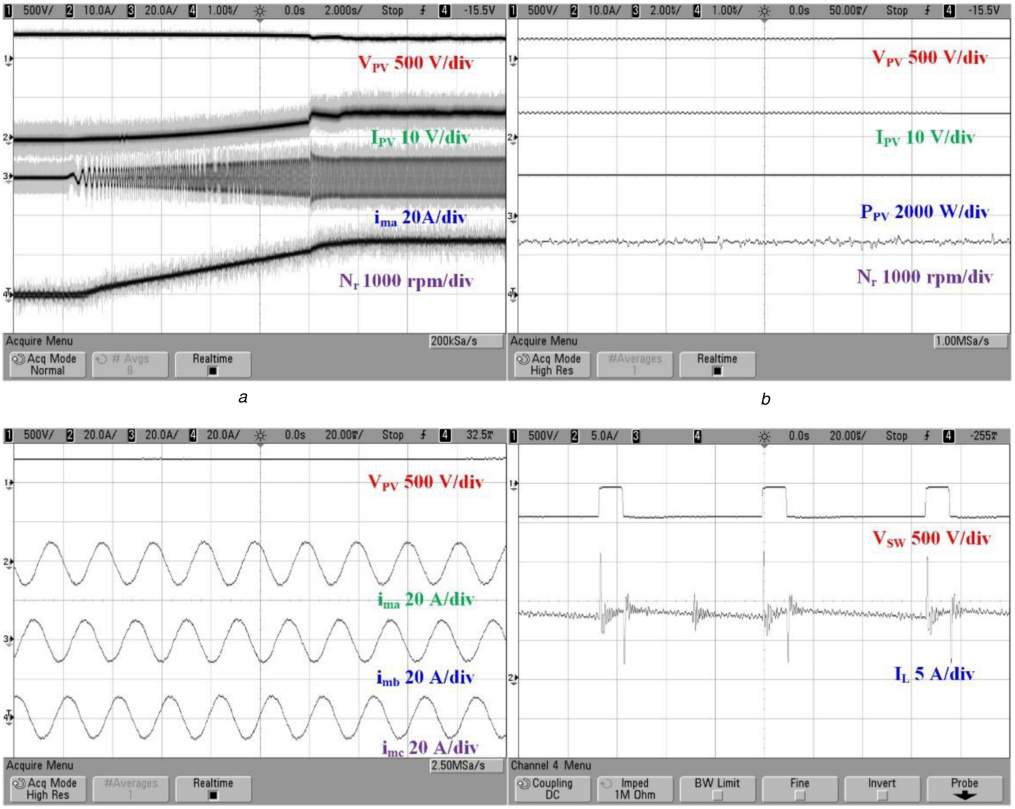

Fig. 3 *Performance of the system in Mode I*
(a) Starting characteristics of the system, *(b)–(d)* Steady state characteristics of the system

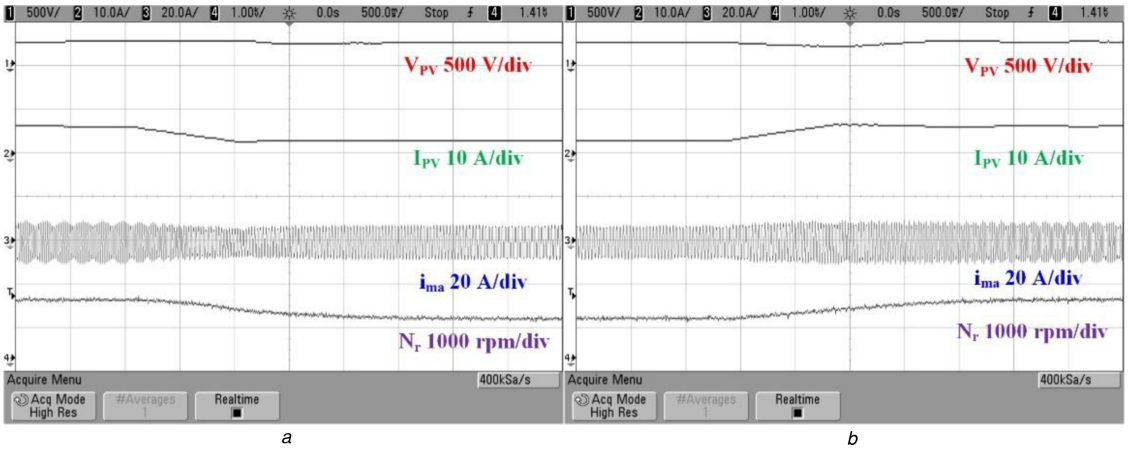

Fig. 4 *Dynamic characteristics of the system in Mode I with radiation change from*
(a) 800 to 500 W/m^2, ***(b)*** 500 to 800 W/m^2

grid at this insolation for rated discharge is 1.31 kW. The distortion in the current is less than 5% even at 50% of rated power testifying the satisfactory PFC operation of the system. Similar, characteristics of the system at radiation of 800 W/m^2 are shown in Figs. 9*c* and *d*. The power drawn from the grid is 588 W and the THD of the input current is 5.7%.

Figs. 10*a* and *b* demonstrate the (P_{PV} vs V_{PV}) and (I_{PV} vs V_{PV}) characteristics of the SPV array. In both the figures, the MPPT efficiency is more than 99%. Moreover, these figures suggest that the system is able to track the MPP even at varying radiation levels. A barchart in Fig. 10*c*, shows the experimental validation of the intelligent sharing of power between the two sources. At an input power of 2.4 kW, the total power output from DC machine is 1.51 kW and hence the efficiency of the emulated volumetric water pump is 63.05%. However, the efficiency of the DC machine is replaced by that of centrifugal pump in the actual system. It is noteworthy here, that the efficiency of highly efficient induction motor is in range of 70–80%. The centrifugal pump's efficiency can be taken as 75%. The overall efficiency of the system can be calculated as, $\eta_{system} = \eta_{mppt} \times \eta_{IM} \times \eta_{pump}$. Therefore, total efficiency of the system is usually of the order of 60%. The usual efficiency of the system is $\eta_{system} = 0.98 \times 0.8 \times 0.75 = 0.588$. The system efficiency can be improved using the motors of higher efficiency (IE4 class). Moreover, super-efficient pumps may also be used which have efficiency of the order of 80%.

7 Conclusion

An intelligent grid interfaced solar water pumping system has been modelled, simulated in MATLAB and experimentally verified in the laboratory. Different modes of operation of the proposed system have been elaborated. The simulated performance of the system at starting, steady state and under dynamic conditions has been validated through the experimental tests. The notable features of the proposed water pumping system are intelligent power sharing, power quality improvement at utility grid supply,

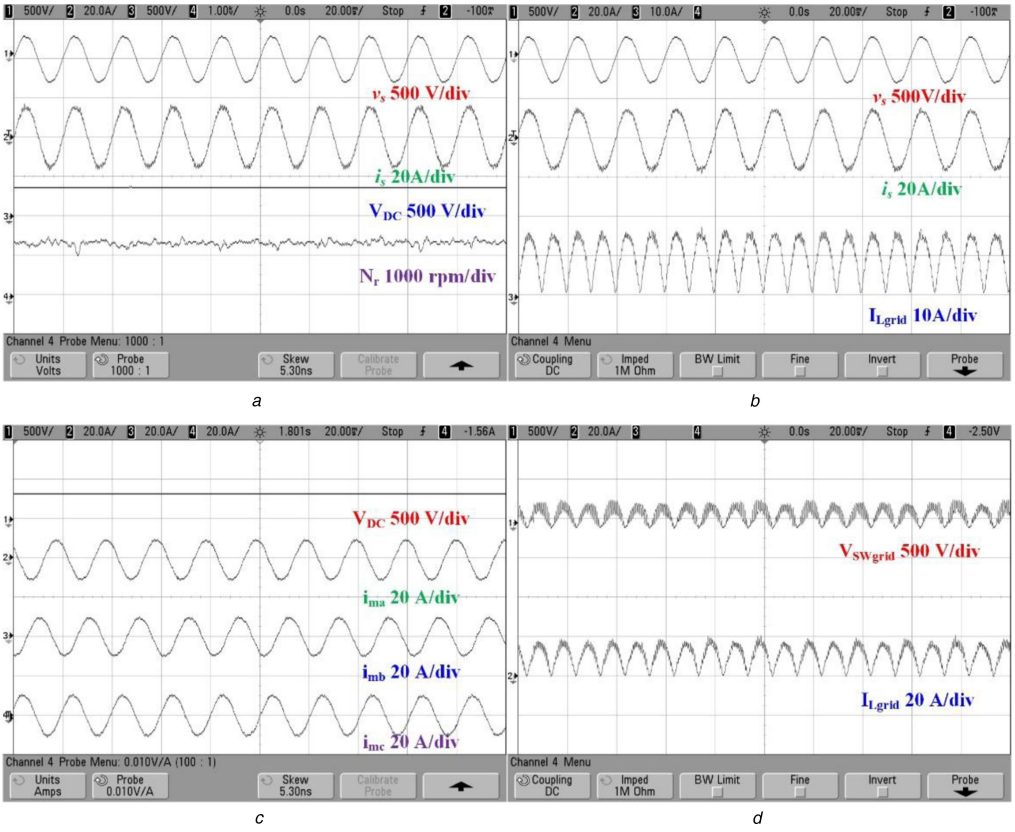

Fig. 5 *Response of the system in Mode II*
(a)–(d) Steady state characteristics of the system in Mode II

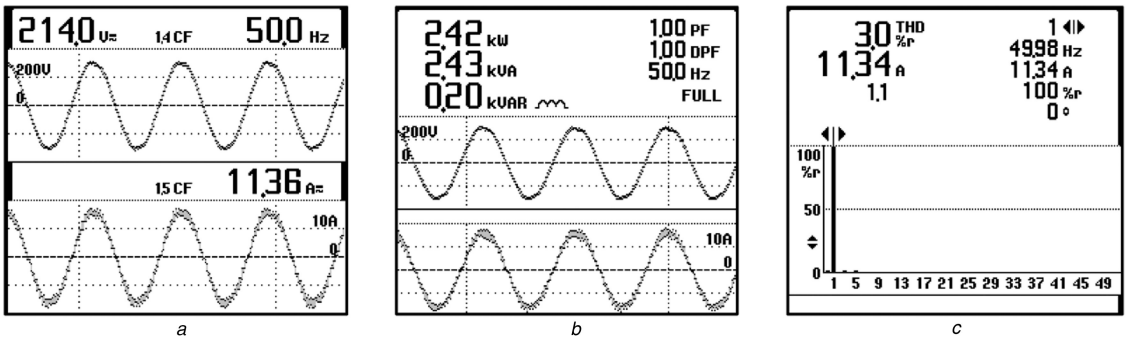

Fig. 6 *Grid parameters with PFC in Mode II*
(a) v_S and i_S, ***(b)*** Grid power, ***(c)*** Harmonic spectrum of i_S

elimination of speed sensor and simple scalar control of induction motor which is easy to implement. Moreover, the system is free from highly inductive transformer element, making it compact and efficient. The system manages to reduce the burden on the utility grid and is helpful in cutting down the electricity bill. The designed control scheme manages to draw maximum available power from SPV array without measuring the ambient temperature and radiation quantitatively. Moreover, irrespective of the available solar radiation, the pump provides the rated discharge, without any interruption in grid interfaced modes of operation. The performance of the proposed system at starting, in steady state and under dynamic conditions is observed to be satisfactory and the system is found suitable for water pumping in irrigation and household applications.

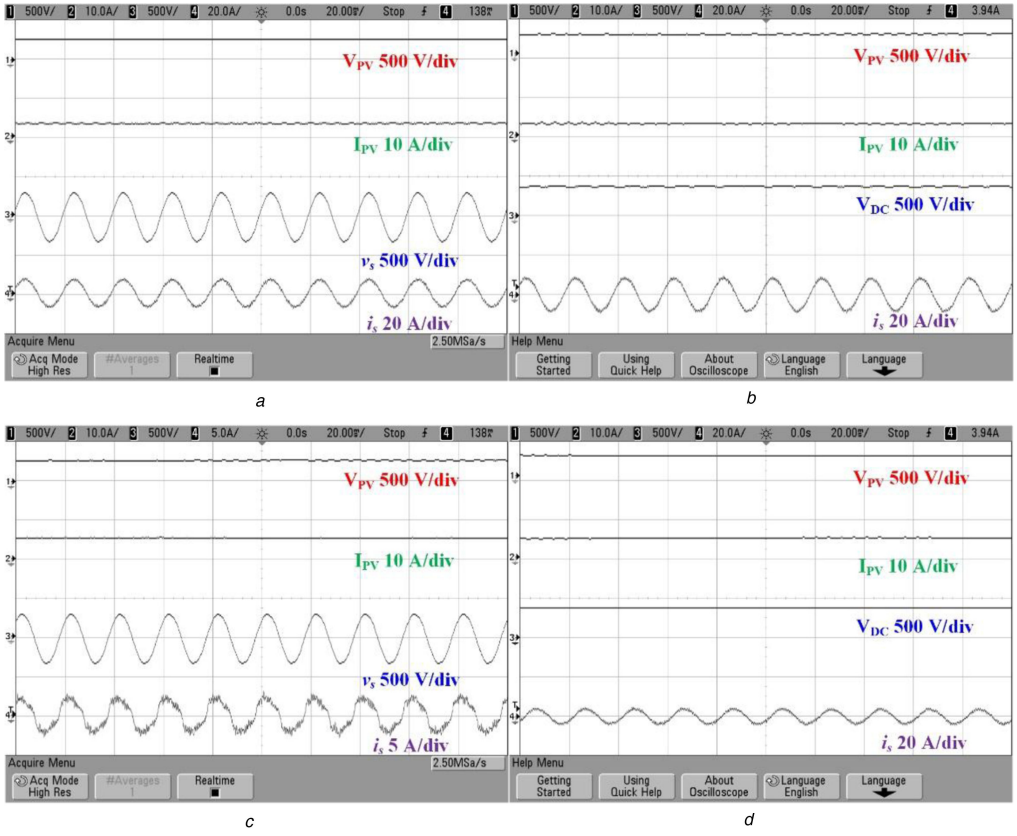

Fig. 7 *Steady state characteristics of the proposed system in Mode III*

(a), ***(b)*** At a radiation of 500 W/m^2, ***(c)***, ***(d)*** At a radiation of 800 W/m^2

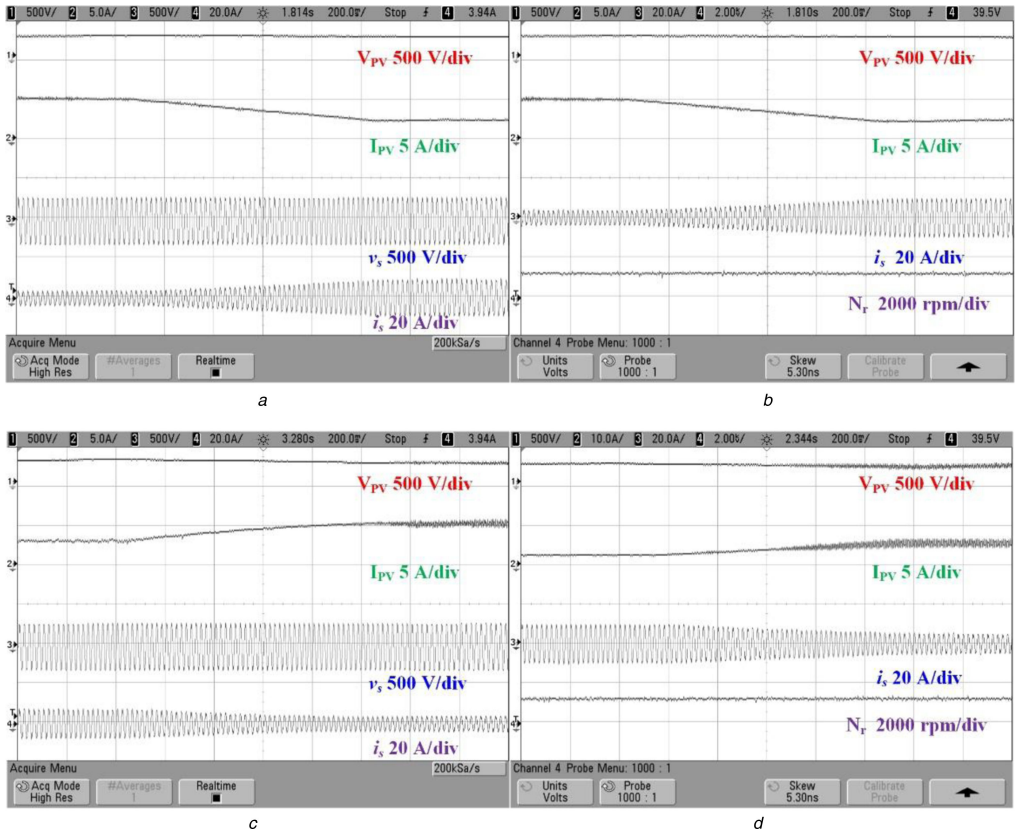

Fig. 8 *Dynamic response of the proposed system in Mode III*

(a), ***(b)*** Variation of system parameters with a decrease in radiation from 800 to 500 W/m^2, ***(c)***, ***(d)*** Variation of system parameters with an increase in radiation from 500 to 800 W/m^2

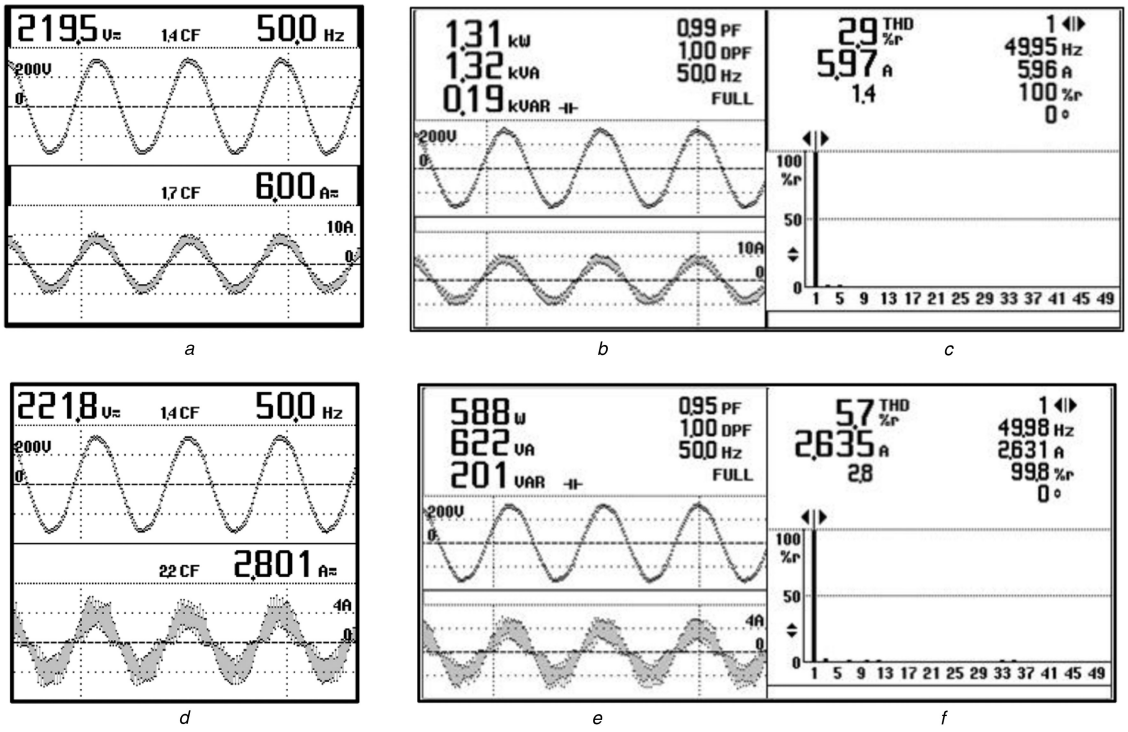

Fig. 9 *Grid parameters with PFC in Mode III*

(***a***) v_S and i_S at 500 W/m^2, ***(b)*** Grid power and harmonic spectrum at 500 W/m^2, ***(c)*** v_S and i_S at 800 W/m^2, ***(d)*** Grid power and harmonic spectrum at 800 W/m^2

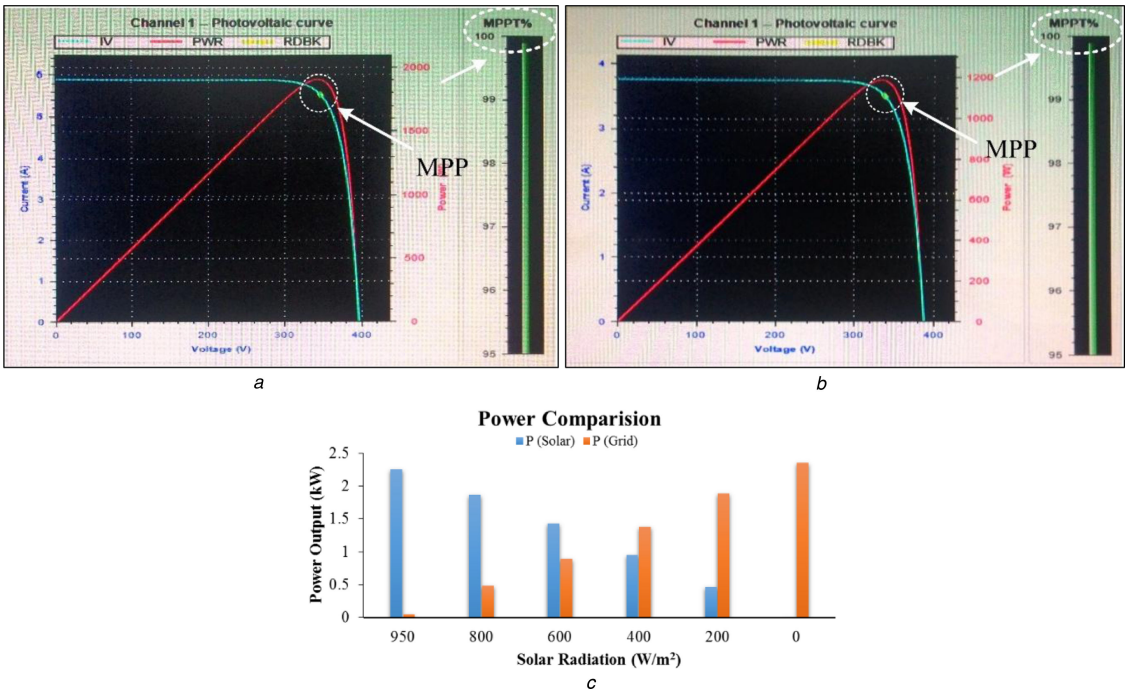

Fig. 10 *Response of the SPV array*

(a) At 800 W/m^2, ***(b)*** At 500 W/m^2, ***(c)*** Sharing of the power between the SPV array and the utility grid

8 References

[1] Smil, V.: '*Power density: a key to understanding energy sources and uses*' (MIT Press, 2015)

[2] Jain, S., Karampuri Somasekhar, V.T.: 'An integrated control algorithm for a single stage PV pumping system using an open end winding induction motor', *IEEE Trans. Ind. Electron.*, 2016, **63**, (2), pp. 956–965

[3] Argaw, N.: '*Renewable energy water pumping systems handbook: period of performance, April 1-September 1, 2001*' (National Renewable Energy Laboratory, 2004)

[4] Thampi, N., Nisha, R.: 'A solar powered water pumping system with efficient storage and energy management', *Int. J. Adv. Res. Electr. Commun. Engg. (IJARECE)*, 2016, **5**, (2), pp. 338–342

[5] Cui, W., Luo, H., Gu, Y., *et al.*: 'Hybrid-bridge transformerless photovoltaic grid-connected inverter', *IET Power Electron.*, 2015, **8**, (3), pp. 439–446

[6] Slabbert, C., Malengret, M.: 'Grid connected/solar water pump for rural areas'. IEEE Int. Symp. on Industrial Electronics, 1998. Proc. ISIE, 1998, vol. **1**, pp. 31–34

[7] Jain, S., Thopukara, A.K., Karampuri, R., *et al.*: 'A single-stage photovoltaic system for a dual-inverter-fed open-end winding induction motor drive for pumping applications', *IEEE Trans. Power Electron.*, 2015, **30**, (9), pp. 4809–4818

[8] Singh, B., Kumar, R.: 'Simple brushless DC motor drive for solar photovoltaic array fed water pumping system', *IET Power Electron.*, 2016, **9**, (7), pp. 1487–1495

[9] Caracas, J.V.M., Farias, G.d.C., Teixeira, L.F.M., *et al.*: 'Implementation of a high-efficiency, high-lifetime, and low-cost converter for an autonomous photovoltaic water pumping system', *IEEE Trans. Ind. Appl.*, 2014, **50**, (1), pp. 631–641

[10] Sharma, U., Dwivedi, S., Jain, C., *et al.*: 'Single stage solar PV array fed field oriented controlled induction motor drive for water pump'. National Power Electronics Conf. (NPEC), IIT Bombay, 2015
[11] Kumar, A., Kochhar, E., Upamanyu, K.: 'Photovoltaic and wind energy hybrid sourced voltage based indirect vector controlled drive for Water Pumping System'. IEEE Int. Conf. on Electrical, Computer and Communication Technologies (ICECCT), Coimbatore, 2015, p. 15
[12] Paz, F., Ordonez, M.: 'High-performance solar MPPT using switching ripple identification based on a lock-in amplifier', *IEEE Trans. Ind. Electron.*, 2016, **63**, (6), pp. 3595–3604
[13] Elgendy, M.A., Atkinson, D.J., Zahawi, B.: 'Experimental investigation of the incremental conductance maximum power point tracking algorithm at high perturbation rates', *IET Renew. Power Gener.*, 2016, **10**, (2), pp. 133–139
[14] Kish, G.J., Lee, J.J., Lehn, P.W.: 'Modelling and control of photovoltaic panels utilising the incremental conductance method for maximum power point tracking', *IET Renew. Power Gener.*, 2012, **6**, (4), pp. 259–266
[15] Moon, S., Kim, S.-J., Seo, J.-W., *et al.*: 'Maximum power point tracking without current sensor for photovoltaic module integrated converter using Zigbee wireless network', *Int. J. Electr. Power Energy Syst.*, 2014, **56**, pp. 286–297
[16] Paz, F., Ordonez, M.: 'Zero oscillation and irradiance slope tracking for photovoltaic MPPT', *IEEE Trans. Ind. Electron.*, 2014, **61**, (11), pp. 6138–6147
[17] Ishaque, K., Salam, Z., Amjad, M., *et al.*: 'An improved particle swarm optimization (PSO)–based MPPT for PV with reduced steady state oscillation', *IEEE Trans.Power Electron.*, 2012, **27**, (8), pp. 3627–3638
[18] Zurbriggen, I.G., Paz, F., Ordonez, M.: 'Direct MPPT control of PWM converters for extreme transient PV Applications'. IEEE Applied Power Electronics Conf. and Exposition (APEC), 2016, pp. 386–391
[19] Sekhar, V.C., Kant, K., Singh, B.: 'DSTATCOM supported induction generator for improving power quality', *IET Renew. Power Gener.*, 2016, **10**, (4), pp. 495–503
[20] Chaudhari, M.A., Suryawanshi, H.M., Renge, M.M.: 'A three-phase unity power factor front-end rectifier for AC motor drive', *IET Power Electron.*, 2012, **5**, (1), pp. 1–10
[21] Yao, Y., Cosic, A., Sadarangani, C.: 'Power factor improvement and dynamic performance of an induction machine with a novel concept of a converter-fed rotor', *IEEE Trans. Energy Convers.*, 2016, **31**, (2), pp. 769–775
[22] Ferreira, F.J.T.E., Almeida, A.T.de: 'Method for in-field evaluation of the stator winding connection of three-phase induction motors to maximize efficiency and power factor', *IEEE Trans. Energy Convers.*, 2006, **21**, (2), pp. 370–379
[23] Maciel, R.S., Freitas, L.C.de, Coelho, E.A.A., *et al.*: 'Front-end converter with integrated PFC and DC-DC functions for a fuel cell UPS with DSP-based control', *IEEE Trans. Power Electron.*, 2015, **30**, (8), pp. 4175–4188
[24] Roggia, L., Beltrame, F., Baggio, J.E., *et al.*: 'Digital current controllers applied to the boost power factor correction converter with load variation', *IET Power Electron.*, 2012, **5**, (5), pp. 532–541
[25] Duarte, J., Lima, L.R., Oliveira, L., *et al.*: 'Single-stage high power factor step-up/step-down isolated AC/DC converter', *IET Power Electron.*, 2012, **5**, (8), pp. 1351–1358
[26] 'IEEE Recommended Practice and Requirements for Harmonic Control in Electric Power Systems - Redline', IEEE Std 519-2014 Revis. IEEE Std 519-1992 - Redline, 2014, pp. 1–213
[27] Bist, V., Singh, B.: 'PFC Cuk converter-fed BLDC motor drive', *IEEE Trans. Power Electron.*, 2015, **30**, (2), pp. 871–887
[28] Wiegand, H.A., Eddy, L.B.: 'Characteristics of centrifugal pumps and compressors which affect the motor driver under transient conditions', *Trans. Am. Inst. Electr. Eng. II Appl. Ind.*, 1960, **79**, (3), pp. 150–156
[29] Vlatkovic, V., Borojevic, D., Lee, F.C.: 'Input filter design for power factor correction circuits', *IEEE Trans. Power Electron.*, 1996, **11**, (1), pp. 199–205
[30] Hussein, K.H., Muta, I., Hoshino, T., *et al.*: 'Maximum photovoltaic power tracking: an algorithm for rapidly changing atmospheric conditions', *IEE Proc. – Gener. Transm. Distrib.*, 1995, **142**, (1), pp. 59–64
[31] Freeland, S.: 'Input current shaping for single phase AC-DC power converters'. *Ph.D. Thesis*, California Institute of Technology, 1988

9 Appendix

2.2 kW(3HP), 230 V, 8.2 A, 50 Hz three phase, 1430 rpm, 4 pole, $R_s = 0.603\ \Omega$, $R_r = 0.7\ \Omega$, $X_s = 1.007\ \Omega$, $X_r = 0.9212\ \Omega$, $X_m = 23.56\ \Omega$.